INTERNATIONAL JOURNAL FOR NUMERICAL METHODS IN FLUIDS
Int. J. Numer. Meth. Fluids 2007; **53**:827–849
Published online 2 August 2006 in Wiley InterScience (www.interscience.wiley.com). DOI: 10.1002/fld.1307

Further application of hybrid solution to another form of Boussinesq equations and comparisons

K. S. Erduran*, †

Hydraulic Division, Civil Engineering Department, Faculty of Engineering and Architecture, University of Nigde, 51100 Nigde, Turkey

SUMMARY

Recently, a new hybrid scheme is introduced for the solution of the Boussinesq equations. In this study, the hybrid scheme is used to solve another form of the Boussinesq equations. The hybrid solution is composed of finite-volume and finite difference method. The finite-volume method is applied to conservative part of the governing equations, whereas the higher order Boussinesq terms are discretized using the finite-difference scheme. Fourth-order accuracy is provided in both time and space. The solution is then applied to several test cases, which are taken from the previous studies. The results of this study are compared with experimental and theoretical results as well as those of the previous ones. The comparisons indicate that the Boussinesq equations solved here and in the previous study produce quite similar results. Copyright © 2006 John Wiley & Sons, Ltd.

Received 8 April 2006; Revised 13 June 2006; Accepted 19 June 2006

KEY WORDS: hybrid scheme; Boussinesq equations (BN & MS); fourth-order accuracy; finite-volume; finite difference; comparisons

1. INTRODUCTION

Starting from Boussinesq [1], many attempts are made to provide a good description of wave propagation from deep to shallow water. The equations describing this phenomenon are named after Boussinesq [1] and called Boussinesq equations. To extent the range of applicability of the original equations, which are developed for a horizontal bottom, Peregrine [2] re-derives a system of Boussinesq equations for varying water depth. Further improvements are made in order to provide a set of equations for deeper water. Madsen *et al.* [3] introduce a new form of equations with improved linear shoaling and dispersive characteristics. Later, Madsen and Sørensen [4] derive a

*Correspondence to: K. S. Erduran, Hydraulic Division, Civil Engineering Department, Faculty of Engineering and Architecture, University of Nigde, 51100 Nigde, Turkey.
†E-mail: kserduran@nigde.edu.tr

new set of equations for slowly varying bathymetry. Beji and Nadaoka [5] also introduce a similar set of equations but their equations differ from Madsen and Sørensen in terms of the way of the derivation of the governing equations. As a result, their momentum equations are different. Nwogu [6] derive another commonly used set of equations in terms of the velocity at arbitrary level. The equations given in References [4–6] describe weak non-linear and weak dispersive water waves in variable water depths and are proved to provide a reasonably good description of wave propagation in coastal regions [7]. In the literature, there are other Boussinesq-type equations such as those given in References [8, 9].

Although there are many forms of the Boussinesq equations, the Boussinesq equations derived by Madsen and Sørensen [4], Beji and Nadaoka [5] and Nwogu [6] are commonly preferred for modelling wave propagation from deep to shallow water [10–13].

As well as the significant developments in the extension of the range of applicability of the Boussinesq-type equations, a considerable amount of studies has been completed in the direction of the solution of these equations. The Boussinesq-type equations are mostly solved by the finite difference method [3–5, 13–15]. The use of finite element method comes next [9–11, 16, 17]. Although the finite-volume method with a shock capturing scheme is widely preferred for the simulation of shallow water [18–21], its application for the Boussinesq-type equations is limited [12, 22]. The solutions given in these two references are also not fully based on the finite-volume method. They are mixture of the finite-volume and the finite-difference methods, so they are called hybrid solutions. The main possible reason for the restriction of the use of the method could be the problem of obtaining characteristics of the equations, which are needed for the estimation of the numerical fluxes through the cell interfaces. Hence, part of the equations is recast in the form that the finite-volume method is applicable and the remaining terms are discretized using the finite-difference method [12].

It has been shown that the applications of all the methods mentioned produce quite accurate results and each of them can be used for the solution of the Boussinesq equations [3–5, 10, 11]. However, it may be stated that the finite-difference method is easiest to use and the finite-element method is more easily applied to irregular domain. The advantages of the finite-volume method over the others are proved for the solution of the shallow water equations [21, 23] but not for the solution of the Boussinesq equations as yet not a solution existed based on entirely-finite volume method. These advantages given in References [21, 23] are briefly as follows: the finite-volume method can be easily applied to structured or unstructured grids and it requires significantly less computational effort than the finite element method. The application of the hybrid solution shows that it gives more accurate results than the finite-difference solution for initially steep wave propagation [22]. Moreover, it has an advantage over the finite-difference method that non-linear convective momentum term is easily treated. The solution is particularly useful for the short and long wave interactions as the solution can be easily turned into entirely finite-volume solution of the shallow water equations by removing so called higher order Boussinesq terms [12].

In this study, previously introduced hybrid solution by Erduran *et al.* [12] for the Boussinesq equations given by Madsen and Sørensen [4] is applied to another form of Boussinesq equations derived by Beji and Nadaoka [5]. Here after, the Boussinesq equations introduced by Madsen and Sørensen [4] are called ‘MS’ and the Boussinesq equations derived by Beji and Nadaoka [5] are named as ‘BN’.

Erduran *et al.* [12] show that the first step in the construction of the hybrid scheme is to recast the governing equations to obtain a conservative part that suits the finite-volume discretization.

DOI: 10.1002/fld

The conservative part has the continuity equation and part of the momentum equations (acceleration term and convective momentum terms). The remaining terms in the momentum equations, namely the higher order dispersive non-linear Boussinesq terms, the friction and the bottom slope terms, are considered as the source and the sink terms. The conservative part is discretized using the finite-volume method with the Roe scheme [24] whereas the source and sink terms are discretized using the finite-difference method.

In order to avoid the numerical diffusion (occurring when the truncation errors are of the same order as the dispersive terms), one way is to provide higher order accuracy [25]. The hybrid method provides fourth-order accuracy in both space and time discretization [12]. The spatial derivative terms in the conservative part are discretized by so-called fourth-order accurate compact monotone upstream-centred schemes for conservation laws (MUSCL)-total variation diminishing (TVD) scheme [26]. The remaining spatial derivative terms are discretized by the ordinary finite-difference approach. The bottom slope term is treated using the surface gradient method, introduced by Zhou *et al*. [20]. A fourth-order accurate solution in time is also provided by using the third-order predictor scheme of Adams–Basforth first and later the fourth-order corrector scheme of Adams–Moulton [25]. In this hybrid solution, the continuity equation is solved explicitly, whereas the momentum equation is solved implicitly, using a double-sweep algorithm [27].

This study has twofold; an application of hybrid scheme to the BN type Boussinesq equations, and a comparison of the results obtained from the solution of the BN and the MS. The present results are also compared with the available experimental and theoretical results.

It is hoped that the comparison would be useful to determine the differences of these equations as both sets of equations (BN and MS) are solved by using the hybrid scheme. The differences (if any) tried to highlight here are only corresponding to practical numerical applications and do not include the derivations of these equations and so forth. In the literature, there are a number of discussions corresponding to the instinctive differences between the MS and the BN. When Beji and Nadaoka [5] first introduce their set of Boussinesq equations, they state that their derivation satisfies the energy conservation but the MS does not. They remark that the differences between the MS and the BN come from the fact that the former uses the depth-integrated velocity whereas the latter uses the mean velocity in their derivations. This leads to different momentum equations with respect to the depth-gradient terms. Later, Schäffer and Madsen [28] claim that the formalism of the BN and the MS are equivalent and the difference is in the implicit choice of bottom slope terms. They state that the shoaling for the MS equations is acceptable up to $kh = 3$ while that of the BN is limited up to $kh = 1.7$. Hence, they remark that the conservation of energy is an important issue but if there is no side effect that limits the application range of the equations. They also conclude that a set of equations with no exact energy conservation does not mean that it is a disadvantage but with a slight variation in the energy conservation one can obtain a better shoaling characteristic. In the further discussion by Beji and Nadaoka [29], it is stressed that the formalism of the BN and the MS is not identical but there is a slight but an obvious difference between them. They claim that one can obtain different forms of the equations if the MS's approach is followed, however, their procedure results in a single possible form. Another point emphasized is that the Boussinesq equations derived based on the mean velocity result in the continuity equation that is exact to all order of dispersion parameters whereas those constructed based on the surface velocity produce the momentum equations, which are exact to all order of dispersion parameters. Therefore, the former generates the truncation errors in the momentum equations while the latter in the continuity equation [29]. However, they claim that it is the reason why the Boussinesq equations formulated in terms of the mean or surface velocity are more accurate than the others, which are said to have

DOI: 10.1002/fld

the truncation errors in both in the continuity and the momentum equations. Later, Schäffer and Madsen [30] emphasize that one cannot reach a conclusion that the Boussinesq equations with either the continuity or the momentum equations exact in a linear sense are more accurate without considering overall accuracy of the combination of these two equations. Regarding to the energy conservation, Schäffer and Madsen [30] also disagree with Beji and Nadaoka [29]. They have highlighted two points; one can conclude that all the formulations conserve the energy within the accuracy that these equations are valid. Secondly, they state that there is no correlation between the energy conservation flux and either the continuity or momentum equations that are exact in a linear sense. During these discussions, Nwogu's equations [6] are also evaluated in terms of the energy conservation. Previously, Nwogu's equations [6] are believed to be in a group of Boussinesq equations that conserve the energy exactly [5], later all contributors to these discussions agree that Nwogu's equations [6] do not also preserve the energy exactly.

Although we have provided brief introductory information on the discussions of the BN and the MS in terms of their instinctive properties, the aim of this study is not to go into this discussion but to introduce the hybrid solution to the BN and to compare the BN and the MS in terms of their practical applications.

In the following section, the BN equations are solved by using the hybrid solution and later in Section 3, the solution is applied to several test cases that are taken from the previous studies. The comparisons are also given in this section. The applicability as well as the observed differences between the BN and the MS are discussed in Section 4. The conclusions are drawn and given in Section 5.

2. METHODOLOGY

In this section, we will first give brief introductory information on the MS. Erduran *et al.* [12] rewrite the MS equations in the following form:

$$\frac{\partial h}{\partial t} + \frac{\partial hu}{\partial x} = 0 \tag{1}$$

$$\frac{\partial hu}{\partial t} + \frac{\partial}{\partial x}\left(hu^2 + \frac{1}{2}gh^2\right) - gh\frac{\partial z}{\partial x} + \psi_x + \frac{\tau_x}{\rho} = 0 \tag{2}$$

$$\psi_x \equiv -\left(\mathrm{B} + \frac{1}{3}\right)d^2\left(\frac{\partial^3 P}{\partial x^2\,\partial t}\right) - \mathrm{B}gd^3\left(\frac{\partial^3 \eta}{\partial x^3}\right) - d\frac{\partial d}{\partial x}\left(\frac{1}{3}\frac{\partial^2 P}{\partial x\,\partial t} + 2\mathrm{B}gd\frac{\partial^2 \eta}{\partial x^2}\right) \tag{3}$$

where η is surface elevation measured from the still water depth (d), P ($P = hu$) is the volume flux, u is the depth-averaged velocity in the x direction, h is the water depth, τ_x is the bottom shear stress in the x direction and B is a coefficient, set equal to $\frac{1}{15}$.

They also show that these equations can be written in compact-conservative form as

$$\frac{\partial \mathbf{q}}{\partial t} + \frac{\partial \mathbf{f}(\mathbf{q})}{\partial x} = \mathbf{b}(\mathbf{q}) \tag{4}$$

where $\mathbf{q} = (h, hu)^{\mathrm{T}}$ is the so-called conservative physical vector; $\mathbf{f}(\mathbf{q}) = (hu, hu^2 + \frac{1}{2}gh^2)^{\mathrm{T}}$ is the flux vector. The vector $\mathbf{b}(\mathbf{q}) = (0, gh(So_x - Sf_x) - \psi_x)^{\mathrm{T}}$ is used to denote the source/sink terms,

DOI: 10.1002/fld

where $So_x = gh(\partial z/\partial x)$ is the bottom slope and Sf_x is the friction term that can be given by Manning's Formula as

$$Sf_x = \frac{n^2 u^2}{h^{4/3}} \tag{5}$$

Now, we try to write the BN equations in a similar compact-conservative form using the same steps that are taken by Erduran *et al.* [12]. The conservative form is necessary for the finite-volume application.

The original BN equations with the bottom shear stress in one-space dimension can be given as

$$\frac{\partial \eta}{\partial t} + \frac{\partial hu}{\partial x} = 0 \tag{6}$$

$$\frac{\partial u}{\partial t} + u\frac{\partial u}{\partial x} + g\frac{\partial \eta}{\partial x} + \psi_x + \frac{\tau_x}{\rho} = 0 \tag{7}$$

$$\psi_x \equiv -(1+\beta)\left[\frac{d^2}{3}\frac{\partial^3 u}{\partial x^2\,\partial t} + d\frac{\partial d}{\partial x}\frac{\partial^2 u}{\partial x\,\partial t}\right] - \beta g\frac{d^2}{3}\frac{\partial^3 \eta}{\partial x^3} - \beta g d\frac{\partial d}{\partial x}\frac{\partial^2 \eta}{\partial x^2} \tag{8}$$

where β is a coefficient and taken to be $\frac{1}{5}$ [5].

Following by Erduran *et al.* [12] to obtain conservative forms of Equations (6) and (7), the following steps should be taken. First, it is assumed that the bottom elevation (topography) is not changing with time or that changes are small in comparison with surface elevation changes, hence:

$$\frac{\partial \eta}{\partial t} = \frac{\partial h}{\partial t} \tag{9}$$

because

$$\frac{\partial \eta}{\partial t} = \frac{\partial (h-d)}{\partial t} = \frac{\partial h}{\partial t} - \frac{\partial d}{\partial t} \quad \text{as } \frac{\partial d}{\partial t} = 0$$

and

$$gh\frac{\partial \eta}{\partial x} = gh\frac{\partial}{\partial x}(h-d) = \frac{\partial}{\partial x}\left(\frac{1}{2}gh^2\right) - gh\frac{\partial d}{\partial x} \tag{10}$$

Second, the derivative of the still water depth, d, with respect to x represents the bottom variation in the x direction. Therefore, it can be rewritten as

$$gh\frac{\partial d}{\partial x} = -gh\frac{\partial z}{\partial x} \tag{11}$$

where z is the bottom elevation measured from the datum. The left-hand side of Equation (11) is known as the bottom slope term.

By introducing Equations (9)–(11) into Equations (6) and (7) and using the following relation [7]:

$$u(x,t) = \frac{P(x,t)}{d(x) + \eta(x,t)} \tag{12}$$

DOI: 10.1002/fld

the new conservative form of the BN equations reads:

$$\frac{\partial h}{\partial t} + \frac{\partial hu}{\partial x} = 0 \tag{13}$$

$$\frac{\partial hu}{\partial t} + \frac{\partial}{\partial x}\left(hu^2 + \frac{1}{2}gh^2\right) - gh\frac{\partial z}{\partial x} + \psi_x + \frac{\tau_x}{\rho} = 0 \tag{14}$$

$$\psi_x \equiv -(1+\beta)\left[\frac{d^3}{3}\frac{\partial^3(Q)}{\partial x^2\,\partial t} + d^2\frac{\partial d}{\partial x}\frac{\partial^2(Q)}{\partial x\,\partial t}\right] - \beta g\frac{d^3}{3}\frac{\partial^3\eta}{\partial x^3} - \beta g d^2\frac{\partial d}{\partial x}\frac{\partial^2\eta}{\partial x^2} \tag{15}$$

where $Q = P/d$.

It can be seen that the difference between the MS and BN is in their momentum equations.

The compact conservative form of the BN reads:

$$\frac{\partial \mathbf{q}}{\partial t} + \frac{\partial \mathbf{f}(\mathbf{q})}{\partial x} = \mathbf{b}(\mathbf{q}) \tag{16}$$

where $\mathbf{q} = (h, hu)^{\mathrm{T}}$ is the so-called conservative physical vector; $\mathbf{f}(\mathbf{q}) = (hu, hu^2 + \frac{1}{2}gh^2)^{\mathrm{T}}$ is the flux vector. The vector $\mathbf{b}(\mathbf{q}) = (0, gh(So_x - Sf_x) - \psi_x)^{\mathrm{T}}$ is used to denote the source/sink terms, where $So_x = gh(\partial z/\partial x)$ is the bottom slope and Sf_x is the friction term that can be given by Manning's Formula as

$$Sf_x = \frac{n^2u^2}{h^{4/3}} \tag{17}$$

Note that the bottom shear stress term is replaced with the friction term.

2.1. Solution

The solution algorithm is chosen exactly as given by Erduran *et al.* [12] in order to provide much better comparisons between the MS and the BN. Therefore, the solution is briefly introduced and the readers refer to Reference [12] for more detailed information.

Equations (13) and (14) are written in the following forms [12, 25]:

$$h_t = E \tag{18}$$

$$U_t = F \tag{19}$$

where

$$U_t = [hu]_t - (1+\beta)\frac{d^3}{3}\left(\frac{P}{d}\right)_{xxt} - (1+\beta)d^2 d_x\left(\frac{P}{d}\right)_{xt}$$

$$E = -[hu]_x$$

$$F = -\left[hu^2 + \frac{1}{2}gh^2\right]_x + ghz_x - ghSf_x + \beta g\frac{d^3}{3}\eta_{xxx} + \beta g d^2 d_x\eta_{xx}$$

and the subscript t denotes time derivative while subscript x denotes space derivative.

DOI: 10.1002/fld

The hybrid scheme is constructed by application of the finite-volume method to the homogeneous part of Equations (16) and the remaining terms are discretized by the finite-difference method. Hence, the overall discretized equations in space read:

$$E = -\frac{1}{A}\sum_{w=1}^{m} \mathbf{T}^{-1}(\theta^w)\mathbf{f}_1^w(\tilde{\mathbf{q}}^w)L^w \tag{20}$$

$$\begin{aligned} F = &-\frac{1}{A}\sum_{w=1}^{m} \mathbf{T}^{-1}(\theta^w)\mathbf{f}_2^w(\tilde{\mathbf{q}}^w)L^w - gh_i\left(\frac{z_{i+1/2}-z_{i-1/2}}{\Delta x}\right) - gh_i Sf_x \\ &+ \frac{\beta g(d_i)^3}{6\Delta x^3}[\eta_{i+2} - 2\eta_{i+1} + 2\eta_{i-1} - \eta_{i-2}] \\ &+ \frac{\beta g(d_i)^2}{12\Delta x^3}(-d_{i+2} + 8d_{i+1} - 8d_{i-1} + d_{i-2})[\eta_{i+1} - 2\eta_i + \eta_{i-1}] \end{aligned} \tag{21}$$

where A is the area of the cell, m is the number of sides of the cell, w is an index that represents the side, $\mathbf{T}(\theta^w)$ is the transformation matrix which can be obtained by rotating the co-ordinate axes, $\mathbf{T}^{-1}(\theta^w)$ is the inverse transformation matrix, L^w is the length of the wth cell side, θ^w is the angle between the outward normal vector $\boldsymbol{n}$ and the x axis, $\tilde{\mathbf{q}}^w$ is the transformed conservative physical (variable) vector obtained by multiplying $\mathbf{q}$ by the transformation matrix and $\mathbf{f}_1^w(\tilde{\mathbf{q}}^w)$ refers to a numerical mass flux, related to the first component, h, $\mathbf{f}_2^w(\tilde{\mathbf{q}}^w)$ corresponds to the numerical momentum flux [18] and $z_{i+1/2}$ and $z_{i-1/2}$ are the bed elevations at cell interfaces; $i+\frac{1}{2}$ and $i-\frac{1}{2}$, respectively [20].

The key element in the finite-volume method is the estimation of the numerical fluxes through the cell interfaces. Again, in order to provide exactly the same solution for the BN, the numerical fluxes are also evaluated using the Roe scheme [24], which is used in the previous study [12] even though the other well-known schemes such as HLL, HLLC and Osher could be applied.

As stated in the introduction section, it is necessary to provide the higher order accuracy to avoid the unwanted numerical diffusion. Thus, the fourth-order compact MUSCL-TVD scheme [26] is used to construct the cell interface values prior to computation of numerical fluxes. The treatment of the bottom slope is achieved by the surface gradient method [20]. As a result, the following equations are obtained for the cell interface values:

$$H_{i+1/2}^{\mathrm{L}} = H_i + [\varphi(r_1)\Delta^* H_{i-1/2} + \varphi(1/r_1)2\Delta^* H_{i+1/2}]/6 \tag{22}$$

$$H_{i+1/2}^{\mathrm{R}} = H_{i+1} - [\varphi(r_2)2\Delta^* H_{i+1/2} + \varphi(1/r_2)\Delta^* H_{i+3/2}]/6 \tag{23}$$

where $H_{i+1/2}^{\mathrm{L}}$ is the surface level at the left-hand side of the interface $i+\frac{1}{2}$ and $H_{i+1/2}^{\mathrm{R}}$ is the surface level at the right-hand side of the interface $i+\frac{1}{2}$.

The inside of the cell under consideration always corresponds to the left-hand side of the interface, and the neighbouring cell to the right-hand side.

The values of $\Delta^* H$ are calculated in the following way:

$$\Delta^* H_{i+1/2} = \Delta H_{i+1/2} - \Delta^3 \overline{H}_{i+1/2}/6, \quad \Delta H_{i+1/2} = H_{i+1} - H_i$$

$$\Delta^3 \overline{H}_{i+1/2} = \Delta \overline{H}_{i+3/2} - 2\Delta \overline{H}_{i+1/2} + \Delta \overline{H}_{i-1/2}$$

DOI: 10.1002/fld

$$\Delta\overline{H}_{i-1/2} = m(\Delta H_{i-1/2}, \Delta H_{i+1/2}, \Delta H_{i+3/2})$$

$$\Delta\overline{H}_{i+1/2} = m(\Delta H_{i+1/2}, \Delta H_{i+3/2}, \Delta H_{i-1/2})$$

$$\Delta\overline{H}_{i+3/2} = m(\Delta H_{i+3/2}, \Delta H_{i-1/2}, \Delta H_{i+1/2})$$

m denotes the Minmod limiter and is given as

$$m(j,k,l) = (S)\max[0, \min(|j|, b_2(S)k, b_2(S)l)]$$

where $S = \text{sign}(j)$ and $b_2 = 2$.

The function $\varphi(r_1)$ for the use of van Leer limiter is defined as

$$\varphi(r_1) = \frac{r_1 + |r_1|}{1 + r_1}$$

and similarly for r_2, where

$$r_1 = \frac{\Delta^* H_{i+1/2}}{\Delta^* H_{i-1/2}}, \quad r_2 = \frac{\Delta^* H_{i+3/2}}{\Delta^* H_{i+1/2}}$$

The construction of cell interface values for h is obtained by

$$h^{\mathrm{L}}_{i+1/2} = H^{\mathrm{L}}_{i+1/2} - z_{i+1/2} \quad \text{and} \quad h^{\mathrm{R}}_{i+1/2} = H^{\mathrm{R}}_{i+1/2} - z_{i+1/2} \tag{24}$$

where $z_i = (z_{i+1/2} + z_{i-1/2})/2$ and $H = h + z$.

The higher order accuracy is also necessary for the time integration and that is provided by using the third-order Adams–Basforth algorithm in the predictor stage and the fourth-order Adams–Moulton algorithm in the corrector stage, resulting in a fourth-order accurate solution in time [12, 25]. The time integration of the BN reads:

(1) Predictor stage (Adams–Basforth method)

$$h^{n+1} = h^n + \frac{\Delta t}{12}[23E^n - 16E^{n-1} + 5E^{n-2}] \tag{25}$$

$$U^{n+1} = U^n + \frac{\Delta t}{12}[23F^n - 16F^{n-1} + 5F^{n-2}] \tag{26}$$

(2) Corrector stage (Adams–Moulton method)

$$h^{n+1} = h^n + \frac{\Delta t}{24}[9E^{n+1} + 19E^n - 5E^{n-1} + E^{n-2}] \tag{27}$$

$$U^{n+1} = U^n + \frac{\Delta t}{24}[9F^{n+1} + 19F^n - 5F^{n-1} + F^{n-2}] \tag{28}$$

U^n and U^{n+1} are given in Equations (29) and (30), respectively.

$$U^n = P^n_i + K1\left[-\frac{P^n_{i+1}}{d^n_{i+1}} + \frac{2P^n_i}{d^n_i} - \frac{P^n_{i-1}}{d^n_{i-1}}\right] + K2\left[-\frac{P^n_{i+1}}{d^n_{i+1}} + \frac{P^n_{i-1}}{d^n_{i+1}}\right] \tag{29}$$

$$U^{n+1} = \left[-\frac{K1}{d^n_{i-1}} + \frac{K2}{d^n_{i-1}}\right] P^{n+1}_{i-1} + \left[1 + 2\frac{K1}{d^n_i}\right] P^{n+1}_i - \left[\frac{K1}{d^n_{i+1}} + \frac{K2}{d^n_{i+1}}\right] P^{n+1}_{i+1} \tag{30}$$

DOI: 10.1002/fld

where $K1=(1+\beta)\,((d_i^n)^3/3\Delta x^2)$ and $K2=(1+\beta)[(d_i^n)^2/24\Delta x^2](-d_{i+2}^n+8d_{i+1}^n-8d_{i-1}^n+d_{i-2}^n)$.

As can be seen, the continuity equation requires an explicit solution, which is obtained from Equations (25) and (27), respectively. However, the momentum equation requires an implicit solution. Hence, Equations (26) and (28) are rearranged and given in Equations (31) and (32).

$$A1P_{i-1}^{n+1}+B1P_i^{n+1}+C1P_{i+1}^{n+1}=D1 \tag{31}$$

$$A1P_{i-1}^{n+1}+B1P_i^{n+1}+C1P_{i+1}^{n+1}=D2 \tag{32}$$

where

$$A1=\left[-\frac{K1}{d_{i-1}^n}+\frac{K2}{d_{i-1}^n}\right],\quad B1=\left[1+2\,\frac{K1}{d_i^n}\right],\quad C1=-\left[\frac{K1}{d_{i+1}^n}+\frac{K2}{d_{i+1}^n}\right]$$

and

$$D1=P_i^n+K1\left[-\frac{P_{i+1}^n}{d_{i+1}^n}+2\,\frac{P_i^n}{d_i^n}-\frac{P_{i-1}^n}{d_{i-1}^n}\right]+K2\left[-\frac{P_{i+1}^n}{d_{i+1}^n}+\frac{P_{i-1}^n}{d_{i-1}^n}\right]$$
$$+\frac{\Delta t}{12}[23F^n-16F^{n-1}-5F^{n-2}]$$

$$D2=P_i^n+K1\left[-\frac{P_{i+1}^n}{d_{i+1}^n}+2\,\frac{P_i^n}{d_i^n}-\frac{P_{i-1}^n}{d_{i-1}^n}\right]+K2\left[-\frac{P_{i+1}^n}{d_{i+1}^n}+\frac{P_{i-1}^n}{d_{i-1}^n}\right]$$
$$+\frac{\Delta t}{24}[9F^{n+1}+19F^n-5F^{n-1}+F^{n-2}]$$

Both in the predictor and the corrector stages, a system of simultaneous linear equations given in Equations (31) and (32) needs to be solved for every grid point. The solution is achieved by using so called 'Double-Sweep algorithm' [26]. However, the corrector stage requires repetition, which ends when the error between two successive results given in Equation (33) is less than 0.001 [25].

$$\Delta f=\frac{\sum_i|f_i^{n+1}-f_i^{(n+1)*}|}{\sum_i|f_i^{n+1}|} \tag{33}$$

where f represents any of the variables (h and P) and $*$ denotes the previous iteration.

3. TESTS AND RESULTS

One of the objectives of this study is to compare the results obtained from the BN and the MS. That's why, the same algorithms introduced by Erduran *et al.* [12] for the solution of the MS is selected. For the same purpose, the hybrid solution of the BN is verified by applying the solution

DOI: 10.1002/fld

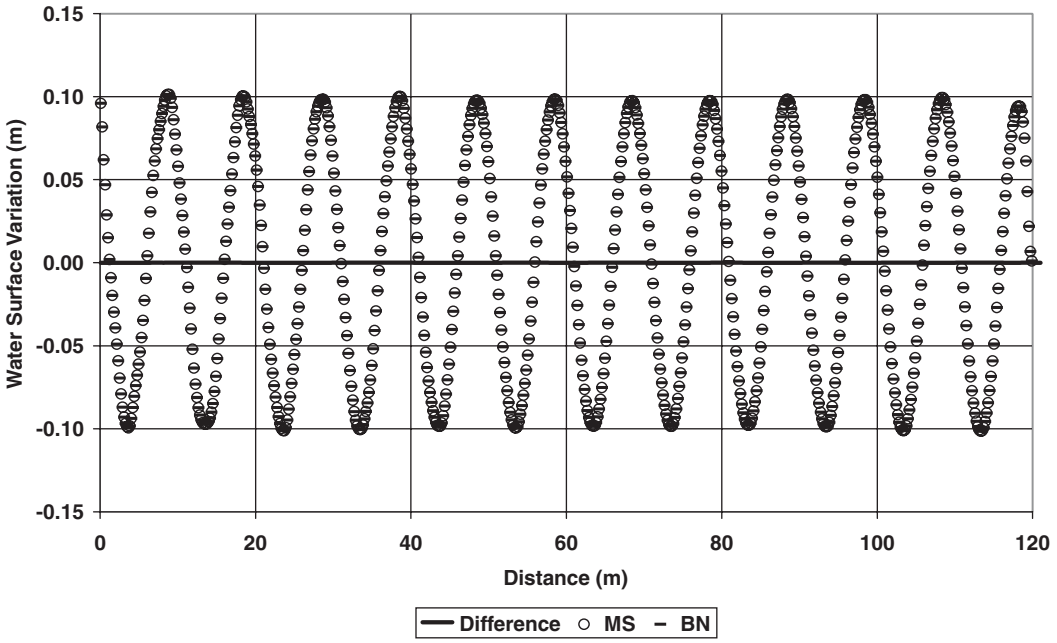

Figure 1. Free surface profiles obtained from MS and BN—sinusoidal wave propagation in deep water ($d/L_0 = 0.43$).

to the tests that used in Reference [12]. These tests are sinusoidal wave propagation in deep waters, bichromatic wave propagation in deep water, sinusoidal wave from deep to shallow water (linear shoaling) and sinusoidal wave propagation over a bar.

3.1. Test A: sinusoidal wave propagation in deep waters

This test is originally given by Madsen *et al*. [3]. In this test, a sinusoidal wave propagates in a channel with a horizontal bottom. The sinusoidal wave amplitude and period are 2.5 s and 0.1 m, respectively, resulting in $d/L_0 = 0.43$ where L_0 is the wave length in deep water. The channel has the still water depth of 4.2 m and it is 120 m long. In the application of the numerical model, at the seaward boundary, a sinusoidal wave is generated and at the shoreward boundary a sponge layer [25, 31] is introduced to absorb the incoming wave. The simulation is completed with a time step of 0.02 s and a spatial grid size of 0.1875 m, resulting in 650 cells being used. The free surface profiles with respect to the still water depth obtained from the present model and the MS given by Erduran *et al.* [12] are shown in Figure 1. This test is repeated in deeper still water depths of 4.5 and 5 m in order to see whether or not the results are influenced with an increase in d/L_0. Figures 2 and 3show the free surface profiles for the still water depths of 4.5 and 5 m, respectively. In Figures 1–3 the continuous line represents the differences in the surface elevation values obtained from the MS and the BN for each grid points. As can be seen from Figures 1–3, the differences for all cases are so small that it is difficult to see them. The computed maximum differences above and below the still water depth for these three cases are given in Table I. The computed and the

DOI: 10.1002/fld

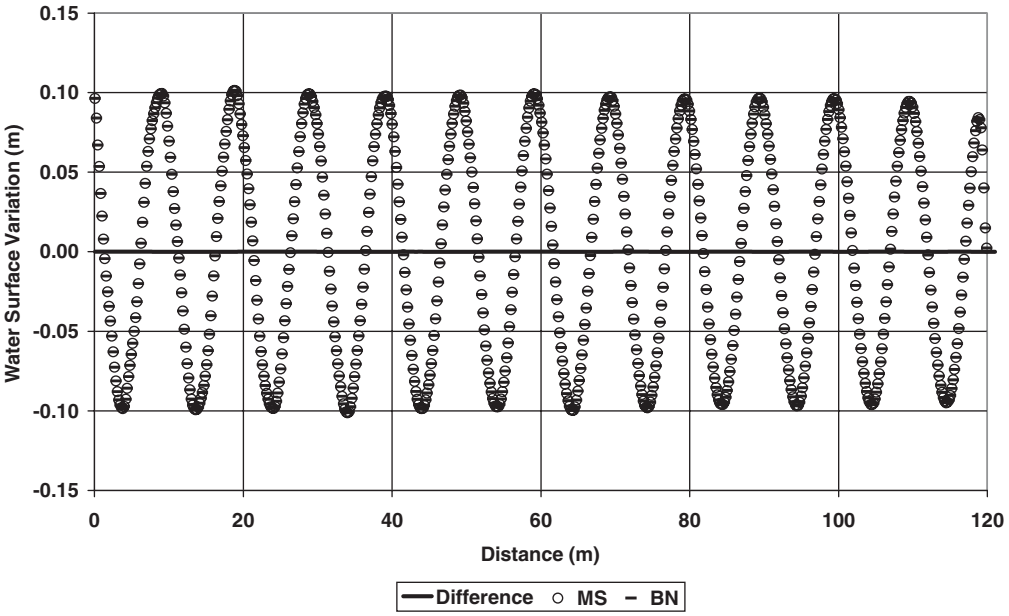

Figure 2. Free surface profiles obtained from MS and BN—sinusoidal wave propagation in deeper water ($d/L_0 = 0.46$).

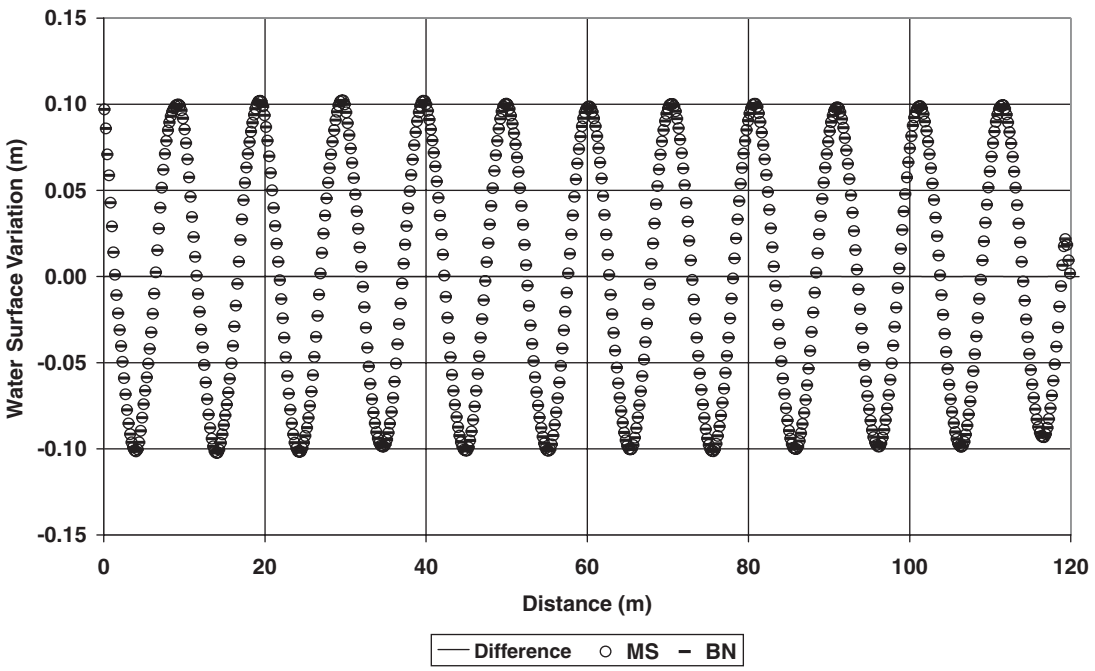

Figure 3. Free surface profiles obtained from MS and BN—sinusoidal wave propagation in deeper water ($d/L_0 = 0.51$).

DOI: 10.1002/fld

Table I. The maximum differences in the surface elevation values obtained from MS and BN for sinusoidal wave propagation in deep water.

d/L_0	The maximum difference above the still water depth (m)	The maximum difference below the still water depth (m)
0.43	6.2×10^{-5}	-3.6×10^{-5}
0.46	4.2×10^{-5}	-5.8×10^{-5}
0.51	4.8×10^{-5}	-5.6×10^{-5}

Table II. Computed and theoretical wavelengths and resulting celerity errors for sinusoidal wave propagation in deep water.

d/L_0	Computed wavelength (m)	Theoretical wavelength (m)	Difference in computed and theoretical wavelength (m)	Celerity errors (%)
0.43	9.97	9.97	9.68	0.29
0.46	10.12	10.12	9.70	0.42
0.51	10.22	10.22	9.73	0.49

theoretical wavelengths obtained from linear wave theory given in Equation (34) are shown in Table II. The differences in wavelengths and the resulting celerity errors are calculated and also given in Table II. As the computed wavelengths obtained from the MS and BN are almost identical, only a single set of computed wavelengths is given in Table II

$$L = \left(\frac{gT^2}{2\pi}\right) \tanh\left(\frac{2\pi d}{L}\right) \tag{34}$$

3.2. Test B: bichromatic wave propagation in deep water

This test is also first introduced by Madsen *et al*. [3]. The same channel, still water depth, time step and the grid size given in the previous test are used. In this test, a wave composed of two sinusoidal waves; one with a period of 2.5 s ($d/L_0 = 0.43$) and another with a period of 3 s ($d/L_0 = 0.3$) are generated at the seaward boundary and the sponge layer is introduced at the shoreward boundary. The amplitude of both waves is 0.05 m. The result at 12 m away from the seaward boundary over 90 s is illustrated in Figure 4. It is again observed that the differences in the surface elevation values obtained from the MS and the BN are unnoticeable with naked eyes. The maximum differences above and below the still water depths are 0.001 and -0.001 m, respectively. The ratio of the maximum differences to the waves heights (0.1 m) are $\pm 1\%$. It is noted that the results presented here agree with those given by Madsen *et al*. [3].

3.3. Test C: sinusoidal wave from deep to shallow water (linear shoaling)

This test is originally used by Madsen and Sørensen [4] and it is conducted in a channel with 700 m long. The bottom of the channel is flat for the first 10 m from the seaward boundary and from 10 to 650 m it has a slope of 1/50 and between 650 and 700 m it is flat again. The constant

DOI: 10.1002/fld

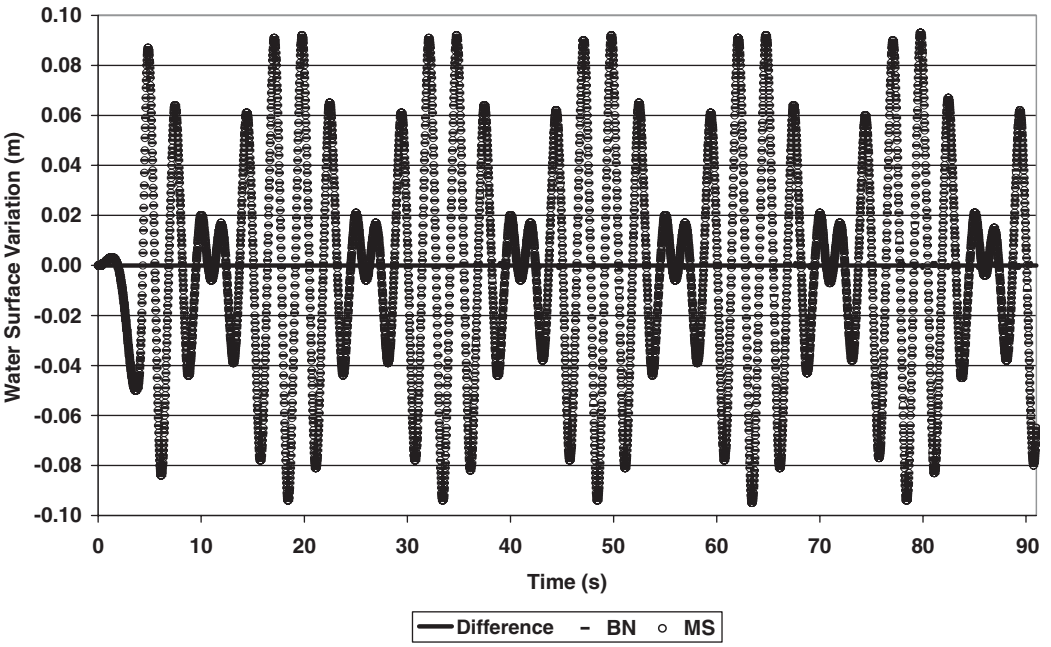

Figure 4. Free surface profiles obtained from MS and BN–bichromatic wave propagation in deep water.

still water depth of 13 m from the seaward boundary to 10 m down is applied whereas the still water depth between 650 and 700 m is 0.2 m. A sinusoidal wave with a period of 4 s is produced at the seaward boundary and again the sponge layer is introduced at the shoreward boundary. The time step and the grid size are chosen exactly the same as taken by Erduran *et al.* [12]. They are 0.01 s and 0.2 m, respectively.

Madsen and Sørensen [4] complete this linear shoaling test by modifying their original momentum equation and they use the following momentum equation instead:

$$\frac{\partial P}{\partial t} + gd\frac{\partial \eta}{\partial x} + \psi_x = 0 \tag{35}$$

As stated by Erduran *et al.* [12], this form of the momentum equation is not suited for the finite-volume application as the slopes of the characteristics cannot be extracted. Therefore, the following momentum equation as introduced by Erduran *et al.* [12] is solved here:

$$\frac{\partial P}{\partial t} + gh\frac{\partial \eta}{\partial x} + \psi_x = 0 \tag{36}$$

Equations (35) and (36) are not the same but it seems that the closest form of Equation (35), which is suited for the finite-volume application, is Equation (36). The problem with hybrid scheme application to Equation (35) is given in more detail in Reference [12].

Figure 5 demonstrates the free surface profiles obtained from the MS and the BN for comparison. As it is difficult to observe the differences between the free surface profiles obtained from the MS

DOI: 10.1002/fld

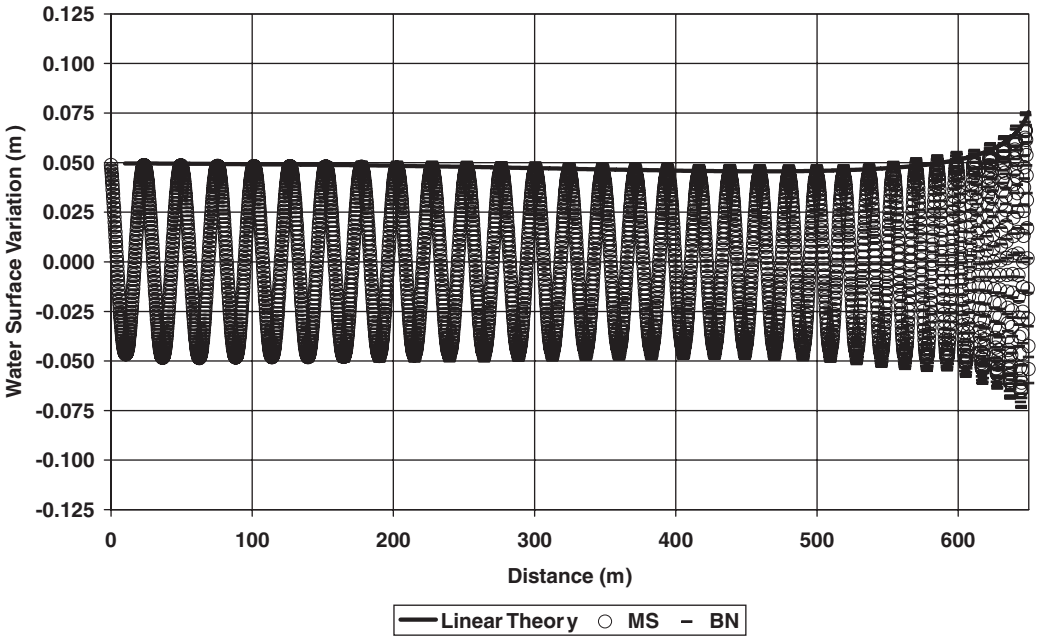

Figure 5. Free surface profiles obtained from MS and BN and maximum elevation envelope calculated by linear theory—sinusoidal wave propagation from deep water to shallow water.

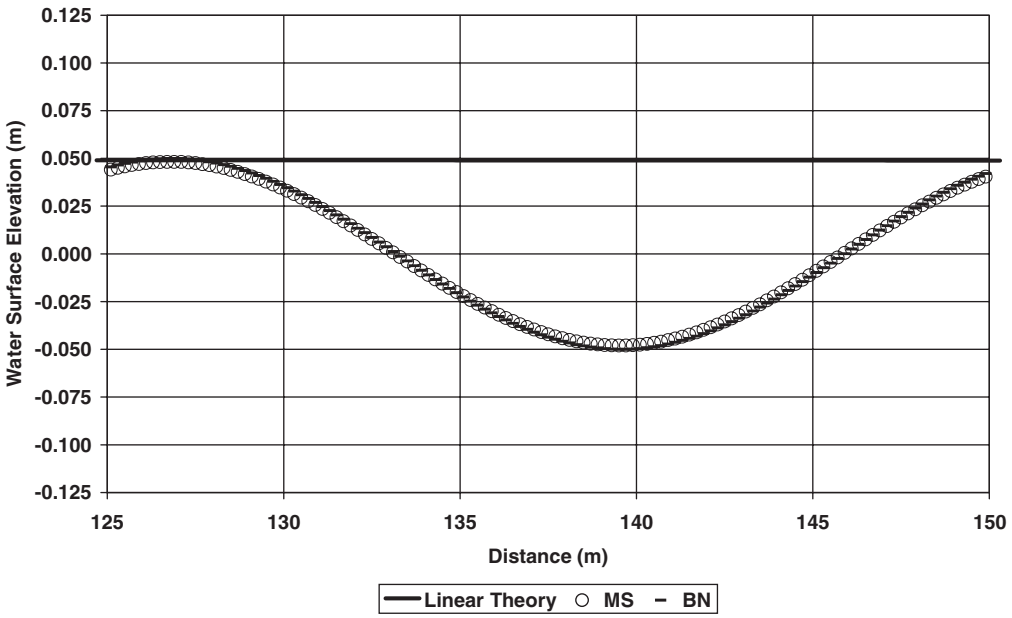

Figure 6. Free surface profiles between 125 and 150 m, obtained from MS and BN and maximum elevation envelope calculated by linear theory—sinusoidal wave propagation from deep water to shallow water.

DOI: 10.1002/fld

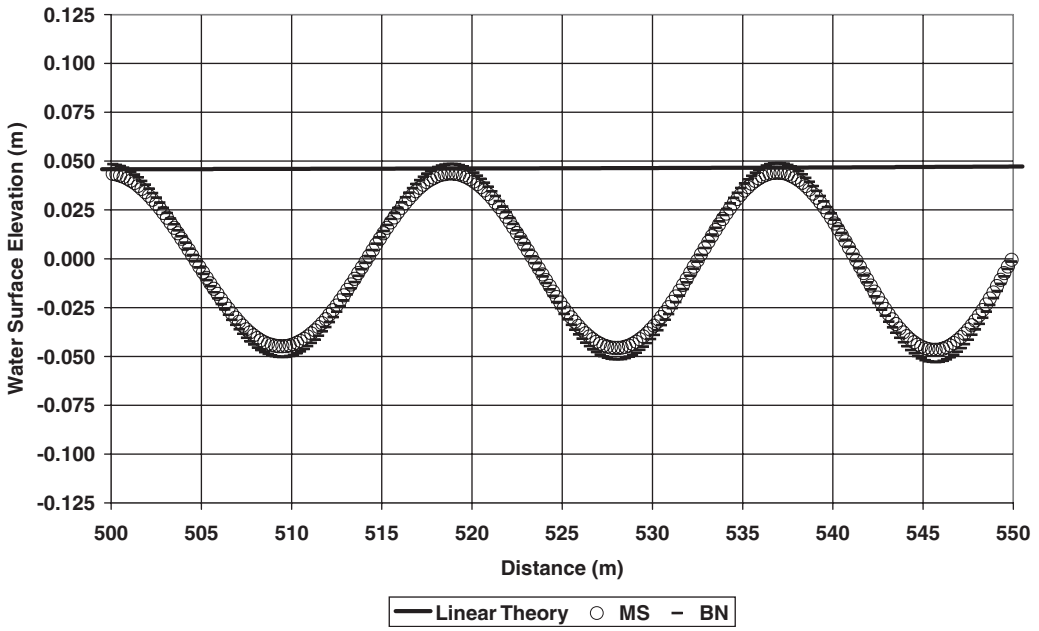

Figure 7. Free surface profiles between 500 and 550 m, obtained from MS and BN and maximum elevation envelope calculated by linear theory—sinusoidal wave propagation from deep water to shallow water.

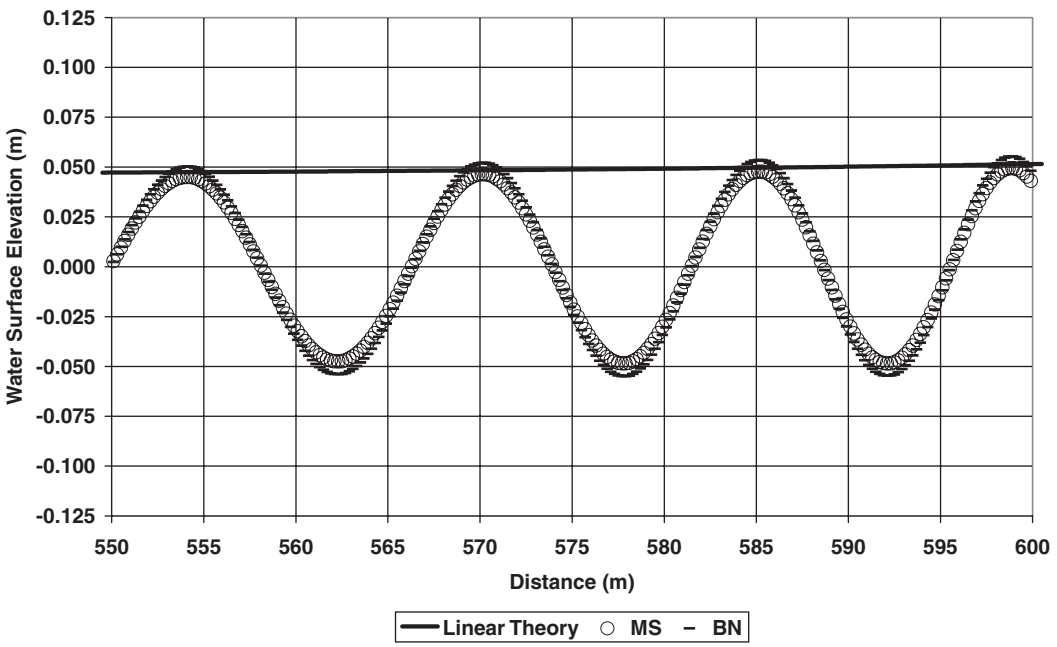

Figure 8. Free surface profiles between 550 and 600 m, obtained from MS and BN and maximum elevation envelope calculated by linear theory—sinusoidal wave propagation from deep water to shallow water.

DOI: 10.1002/fld

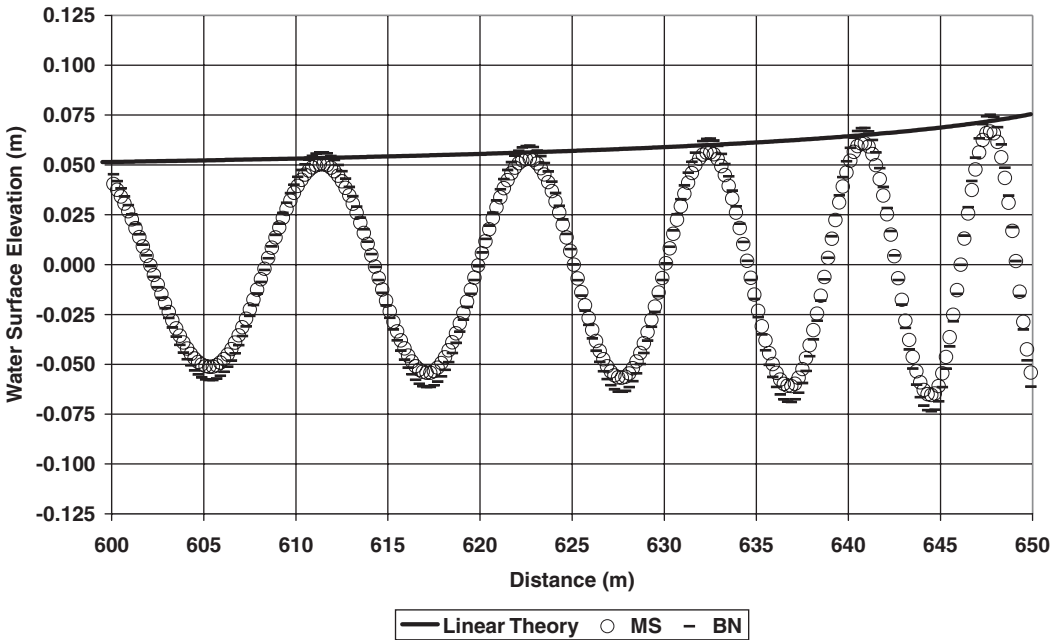

Figure 9. Free surface profiles between 600 and 650 m, obtained from MS and BN and maximum elevation envelope calculated by linear theory—sinusoidal wave propagation from deep water to shallow water.

and the BN due to the presentation of large amount of data, Figures 6–9 showing the same profiles in a smaller interval are provided. In Figures 5–9, the maximum elevation envelope calculated by linear theory is also demonstrated for comparisons of the results. Starting from the beginning, it is observed that both the results of the BN and the MS show small discrepancies comparing to the maximum elevation envelope. Generally speaking, the free surface profile of the BN is above the maximum elevation envelope whereas that of the MS is below. It is also realized that the differences in the surface elevations values obtained from both the BN and the MS with respect to that of the linear theory generally increase towards the shoreward boundary. In order to provide a much better comparison, the peak surface elevation values above the still water depths at wave crests along the channel obtained from the solutions of the BN, MS and the linear theory as well as the differences are given in Table III. Furthermore, the errors in the peak surface elevation values of the BN and the MS are also computed with respect to the linear theory. They are given in Table IV.

It is seen that the MS results are generally closer to the results of the linear theory even though the BN produce better results at some points, see Table IV. This statement is also confirmed by the calculated total absolute differences, computed using the peak values at the wave crests; the total absolute difference between the results of the MS and the linear theory is 0.0617 m and the total absolute difference between the results of the BN and the linear theory is 0.0774 m. The MS produces the maximum error of 7.3% whereas the BN gives 8.1%. The computed averaged errors for the MS and the BN are 3.8 and 5.1%, respectively.

DOI: 10.1002/fld

Table III. Linear shoaling test results: the peak surface elevation values above the still water depths at wave crests along the channel obtained from the solutions of BN, MS and Linear theory and the calculated differences.

Distance (m)	Linear theory	MS solution	BN solution	Difference (m) MS	Difference (m) BN
23.5	0.0496	0.0487	0.0488	0.0009	0.0008
49.7	0.0495	0.0485	0.0491	0.0009	0.0004
75.7	0.0494	0.0483	0.0493	0.0010	0.0001
101.3	0.0492	0.0482	0.0496	0.0010	−0.0004
126.9	0.0491	0.0482	0.0500	0.0009	−0.0009
152.3	0.0489	0.0480	0.0502	0.0009	−0.0013
177.5	0.0487	0.0478	0.0503	0.0008	−0.0017
202.7	0.0484	0.0474	0.0503	0.0010	−0.0019
227.5	0.0482	0.0472	0.0503	0.0010	−0.0022
251.9	0.0479	0.0468	0.0502	0.0011	−0.0024
276.5	0.0476	0.0464	0.0501	0.0012	−0.0026
300.7	0.0472	0.0459	0.0499	0.0013	−0.0026
324.5	0.0469	0.0454	0.0495	0.0015	−0.0026
348.1	0.0466	0.0451	0.0494	0.0015	−0.0028
371.3	0.0463	0.0447	0.0491	0.0017	−0.0028
394.1	0.0461	0.0445	0.0491	0.0016	−0.0031
416.5	0.0459	0.0440	0.0487	0.0018	−0.0028
438.3	0.0457	0.0439	0.0487	0.0018	−0.0030
459.5	0.0457	0.0437	0.0485	0.0020	−0.0029
480.1	0.0457	0.0435	0.0484	0.0022	−0.0027
499.9	0.0459	0.0436	0.0485	0.0023	−0.0027
518.9	0.0462	0.0436	0.0485	0.0026	−0.0023
536.9	0.0467	0.0440	0.0490	0.0027	−0.0023
554.1	0.0474	0.0450	0.0503	0.0024	−0.0028
570.3	0.0484	0.0464	0.0521	0.0020	−0.0037
585.3	0.0497	0.0476	0.0535	0.0020	−0.0039
598.9	0.0513	0.0494	0.0553	0.0020	−0.0040
611.5	0.0535	0.0503	0.0563	0.0032	−0.0028
622.7	0.0563	0.0531	0.0597	0.0033	−0.0034
632.5	0.0600	0.0562	0.0632	0.0038	−0.0032
640.9	0.0651	0.0608	0.0685	0.0043	−0.0034
647.7	0.0720	0.0668	0.0752	0.0052	−0.0032
Total absolute difference (m)				0.0617	0.0774

3.4. Test D: sinusoidal wave propagation over a bar

This test is believed to be a good example to analyse the performance of the short wave models [7, 10, 12]. A bar on a 25 m long channel is situated between 6 and 17 m. In the remaining parts of the channel, the bottom is flat. The bar is introduced by applying an upward slope of 1:20 between 6 and 12 m and steeper downward slope of 1:10 between 14 and 17 m. The top of the bar between 12 and 14 m is horizontal. The depths in horizontal part before and after the bar and in the horizontal part on the top of the bar are 0.4 and 0.1 m, respectively. At the seaward boundary sinusoidal wave with an amplitude of 0.01 m and a period of 2.02 s is generated and at the

DOI: 10.1002/fld

Table IV. Linear shoaling test results: the errors, computed with respect to the linear theory, in the peak surface elevation values above the still water depths at the wave crests along the channel.

Distance (m)	Error in MS (%)	Error in BN (%)
23.5	1.8	1.5
49.7	1.9	0.8
75.7	2.1	0.1
101.3	2.0	−0.8
126.9	1.8	−1.9
152.3	1.8	−2.7
177.5	1.7	−3.5
202.7	2.0	−4.0
227.5	2.1	−4.6
251.9	2.3	−5.1
276.5	2.5	−5.5
300.7	2.8	−5.7
324.5	3.2	−5.8
348.1	3.3	−6.1
371.3	3.6	−6.3
394.1	3.4	−6.9
416.5	4.0	−6.4
438.3	3.9	−6.9
459.5	4.3	−6.6
480.1	4.7	−6.3
499.9	4.9	−6.1
518.9	5.6	−5.3
536.9	5.7	−5.2
554.1	5.0	−6.3
570.3	4.2	−8.0
585.3	4.1	−8.1
598.9	3.8	−8.1
611.5	6.0	−5.6
622.7	5.8	−6.3
632.5	6.3	−5.7
640.9	6.6	−5.7
647.7	7.3	−4.8
Averaged error (%)	3.8	5.1

shoreward boundary, a sponge layer is applied as in the previous tests. The numerical simulation is performed using the same time step of $\Delta t = 0.007$ s and cell size of $0.025\,\text{m} \times 1\,\text{m}$ as given by Erduran *et al.* [12] for comparisons.

The time histories of the free surface profiles at points 10.5, 13.5, 15.7 and 17.3 m are given in Figures 10–13, respectively. The obtained free surface profiles from the solutions of the BN and the MS show a similar trend. However, it appears to be that the results of the BN are slightly better comparing to the experimental ones, particularly at the turning points on the profiles. Overall, both the BN and the MS results are in very good agreement with those obtained from using other numerical techniques [7, 10].

DOI: 10.1002/fld

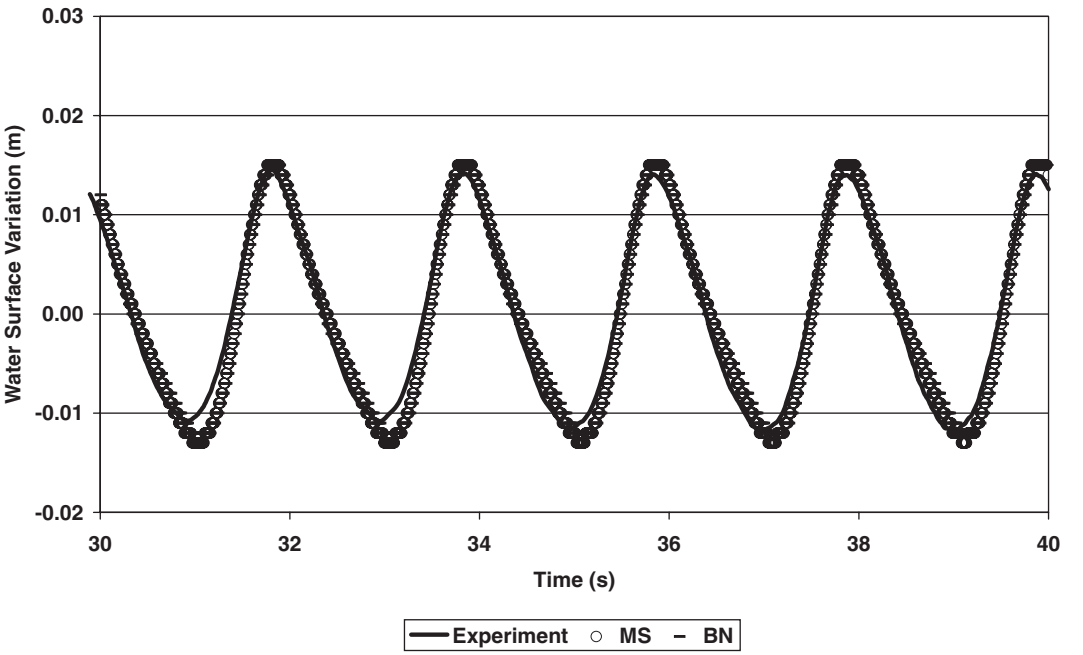

Figure 10. Time histories of free surface profiles obtained from the solutions of the BN and the MS and the experiment at 10.5 m—sinusoidal wave propagation over a bar.

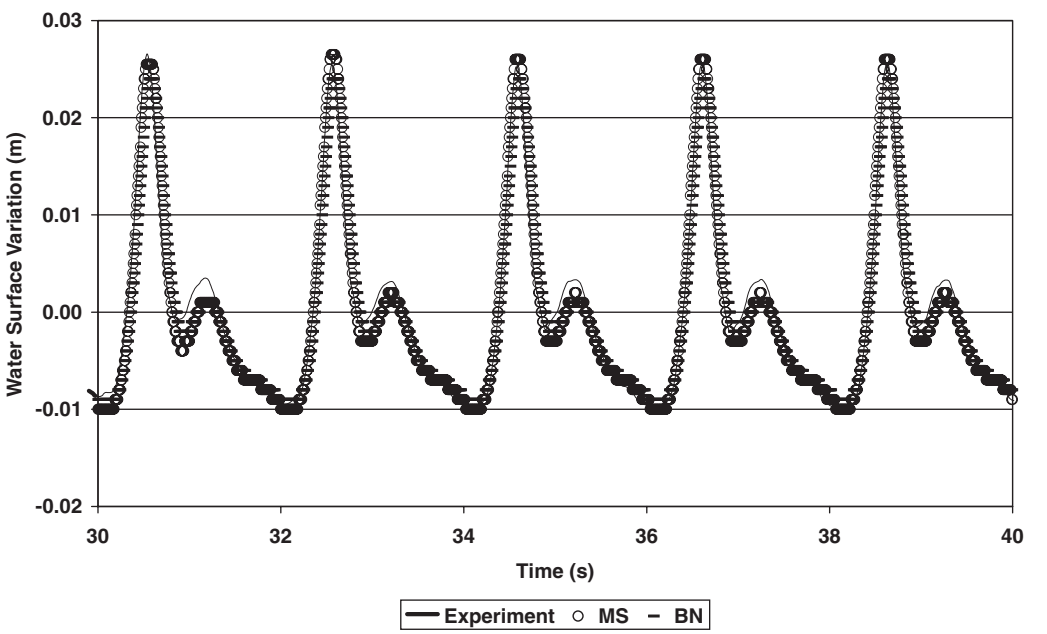

Figure 11. Time histories of free surface profiles obtained from the solutions of the BN and the MS and the experiment at 13.5 m—sinusoidal wave propagation over a bar.

DOI: 10.1002/fld

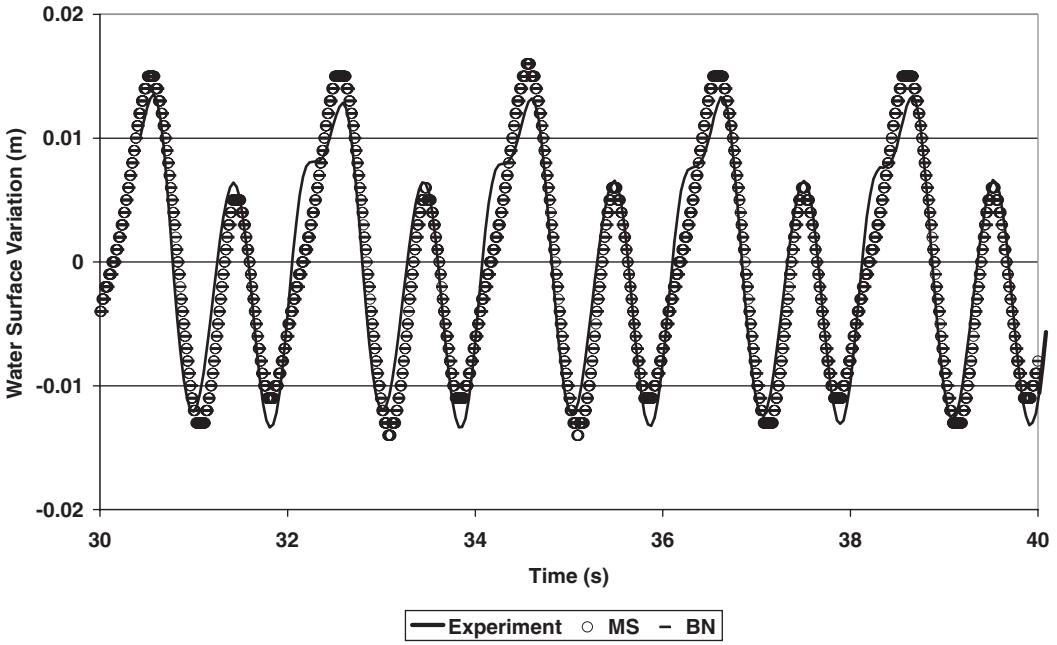

Figure 12. Time histories of free surface profiles obtained from the solutions of the BN and the MS and the experiment at 15.7 m—sinusoidal wave propagation over a bar.

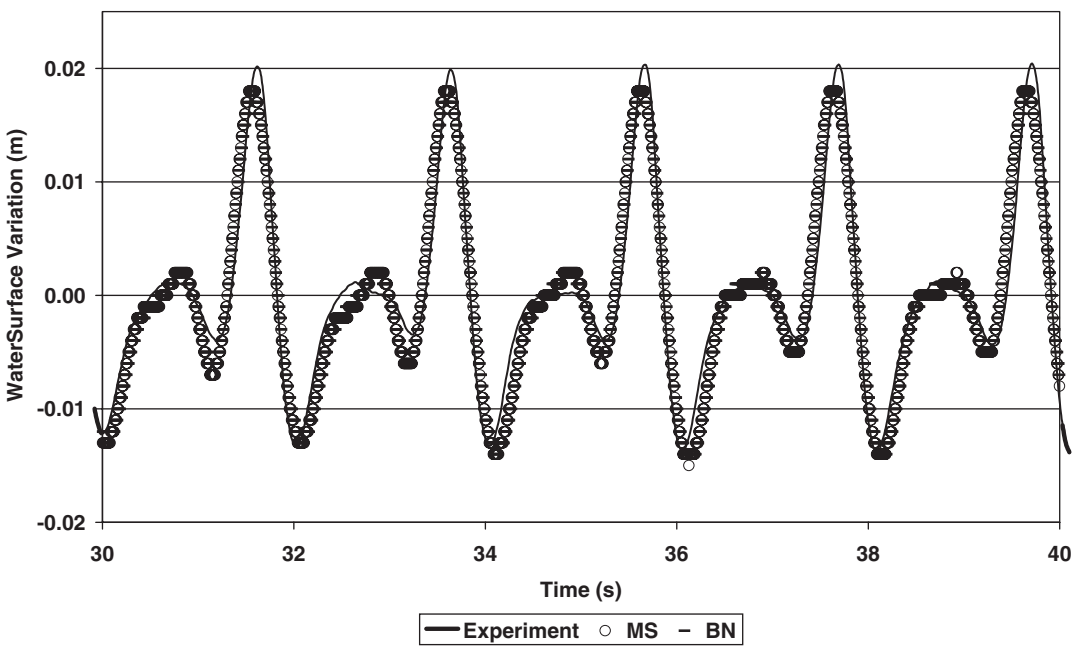

Figure 13. Time histories of free surface profiles obtained from the solutions of the BN and the MS and the experiment at 17.3 m—sinusoidal wave propagation over a bar.

DOI: 10.1002/fld

4. DISCUSSION

Tests A and B indicate that there are almost no differences between the results obtained from the solutions of the BN and the MS, suggesting that their performances for the simulation of deep water wave propagations on a horizontal bottom are identical. The results also suggest that even if the MS type equations produce truncation errors in both in the continuity and the momentum equations as stated by Beji and Nadaoka [29], these errors should be very small or they are almost in the same order of the errors generated by the BN, which is said to have truncation errors only in the continuity equation. Therefore, the results support the statement of Schäffer and Madsen [30] that overall accuracy rather than the accuracy of the continuity or the momentum equations should be checked before reaching a conclusion.

The results of the linear shoaling test also agree with the statement of Schäffer and Madsen [28] that a slight variation in the energy conservation can be an advantage. Even though the BN energy conservation is assumed to be better than the MS, it has been demonstrated that the linear shoaling characteristic of the MS is slightly better. It should be worth remembering that the results obtained in this study is based on the hybrid solution of Equation (36) which is slightly different than Equation (35) originally used by Madsen and Sørensen [4]. Therefore, the computed differences between the MS and the BN obtained from the linear shoaling test may not be the same if Equation (35) instead of Equation (36) could have been solved by the hybrid scheme.

When the results of sinusoidal wave propagation over a bar obtained from the BN and the MS are analysed, it is seen that there are again not obvious differences between them. In fact, the differences do not cause any significant discrepancies on the obtained free surface profiles and comparing to the experimental free surface profile, both the BN and the MS show similar trends. At some points, the BN results are closer to the experimental ones while at some other points the MS results are closer. However, in general, it appears to be the BN results slightly better. This may be due to fact that the truncation errors generated by the BN are less than that of the MS and this property of the BN may not have manifested itself in the sinusoidal wave propagation in deep waters over a horizontal bottom. However, the bar test is believed to be one of the ultimate tests to determine the performances of the short wave models and even from this test it is difficult to conclude that the BN type of the Boussinesq equations is better regarding to the accuracy.

Although it appears to be the results of Tests A, B do not agree with the results of the bar test, considering the size of the differences, one can conclude that both the BN and the MS are equal. Not any significant differences are found to recommend choosing one to another. Both equations can be used for the similar test cases.

Although the aim of this study is not to discuss advantages or disadvantages of the hybrid solution over the readily available entirely finite-element or finite-difference solutions, it may be worth noting that the hybrid solution has a disadvantage over the other methods that the grid size used in all applications has to be chosen smaller. Thus, the time step is also selected to be smaller due to the explicit solution of the continuity equation. This is mainly due to the use of the limiter function used to provide fourth-order accuracy in space [12]. Different slope limiters including Minmod, Superbee, van-Leer, van-Albada, and K limiters were tested but the problem was not yet solved even though slight improvement was obtained with the use of K limiter. Therefore, there is still a need for more research to find the most suitable limiter function. The advantages of the hybrid solution are already given in the introduction section so it is skipped here.

Overall, the results show that both the BN and the MS type Boussinesq equations provide a reasonably good description of wave propagation in coastal regions.

DOI: 10.1002/fld

5. CONCLUSION

The following conclusions can be drawn from this study:

(1) Previously introduced hybrid solution is applied to another form of the Boussinesq equations (BN). The results are compared with the experimental and theoretical results and it has been shown that the hybrid solution of the BN can be used for the short wave simulations.
(2) BN and MS type Boussinesq equations are compared and apart from the linear shoaling test results the comparisons show that they produce almost identical results, indicating that the order of the truncation errors (if any) generated by the use of the BN or the MS type Boussinesq equations should be almost the same. If there is any correlation between the truncation errors and the exact energy conservation, then it may be concluded that their energy conservation properties should also be similar or they are not distinguishable within the accuracy that these equations valid as stated by Schäffer and Madsen [30].
(3) The linear shoaling characteristics of the MS is found to be slightly better but looking at the averaged errors (3.8% for the MS and 5.1% for the BN), one can argue that the hybrid solution of the BN could also be used in similar flow conditions.
(4) Overall, the author believes that both the BN and the MS can be used for the simulation of the short wave propagations and it is difficult to suggest one over another.

ACKNOWLEDGEMENTS

This work is initiated on the basis of the previous study that the author worked with. Therefore, the author would like to thank Dr Susana Ilic and Dr Vedrana Kutija for their contributions on the first development of the hybrid solution and the author would like to thank Prof. M. W. Dingemans for providing the experimental results used here and the previous work. Finally, the author would also like to thank the U.K. Engineering and Physical Sciences Research Council (EPSRC) for their financial support on the previous work.

REFERENCES

1. Boussinesq J. Théorie des ondes et des ramous qui se propagent le long d'un canal rectangulaire horizontal. *Journal de Mathématique Pures et Appliquées*, deuxiéme série 1872; **17**:55–108.
2. Peregrine DH. Long waves on a beach. *Journal of Fluid Mechanics* 1967; **27**:815–827.
3. Madsen PA, Murray R, Sørensen OR. A new form of the Boussinesq equations with improved linear dispersion characteristics. *Coastal Engineering* 1991; **15**:371–388.
4. Madsen PA, Sørensen OR. A new form of the Boussinesq equations with improved linear dispersion characteristics. Part 2. A slowly-varying bathymetry. *Coastal Engineering* 1992; **18**:183–204.
5. Beji S, Nadaoka K. A formal derivation and numerical modelling of the improved Boussinesq equations for varying depth. *Ocean Engineering* 1996; **23**:691–704.
6. Nwogu O. Alternative form of Boussinesq equations for nearshore wave propagation. *Journal of Waterway, Port, Coastal, and Ocean Engineering* 1993; **119**:618–638.
7. Dingemans M. *Water Wave Propagation over Uneven Bottoms*. Advance Series in Ocean Engineering, vol. 13. Part 2. World Scientific: Singapore, 1997.
8. Wei G, Kirby JT, Grilli ST, Subramanya R. A fully nonlinear Boussinesq model for surface waves. Part 1: Highly nonlinear unsteady waves. *Journal of Fluid Mechanics* 1995; **294**:71–92.
9. Zhao M, Teng B, Cheng L. A new form of generalized Boussinesq equations for varying water depth. *Ocean Engineering* 2004; **31**:2047–2072.
10. Walkley M, Berzins M. A finite element method for the one-dimensional extended Boussinesq equations. *International Journal for Numerical Methods in Fluids* 1999; **29**:143–157.

DOI: 10.1002/fld

11. Walkley M, Berzins M. A finite element method for the two-dimensional extended Boussinesq equations. *International Journal for Numerical Methods in Fluid*s 2002; **39**:865–885.
12. Erduran KS, Ilic S, Kutija V. Hybrid finite-volume finite difference scheme for the solution of Boussinesq equations. *International Journal for Numerical Methods in Fluid*s 2005; **49**:1213–1232.
13. Li YS, Zhan JM. Boussinesq-type model with boundary-fitted coordinate system. *Journal of Waterway*, *Port*, *Coastal*, *and Ocean Engineering* 2001; **127**:152–160.
14. Abbott MB, McCowan AD, Warren IR. Accuracy of short-wave numerical models. *Journal of Hydraulic Engineering* 1984; **110**:1287–1301.
15. Karambas ThV, Koutitas C. A breaking wave propagation model based on the Boussinesq equations. *Coastal Engineering* 1992; **18**:1–19.
16. Kawahara M, Cheng JY. Finite element method for Boussinesq wave analysis. *International Journal of Computational Fluid Dynamics* 1994; **2**:1–17.
17. Li YS, Liu S-X, Yu Y-X, Lai G-Z. Numerical modeling of Boussinesq equations by finite element method. *Coastal Engineering* 1999; **37**:97–122.
18. Erduran KS, Kutija V, Hewett CJM. Performance of finite-volume solutions to the shallow water equations with shock-capturing schemes. *International Journal for Numerical Methods in Fluids* 2002; **40**:1237–1273.
19. Brufau P, Vázquez-Cendon ME, García-Navarro P. A numerical model for the flooding and drying of irregular domains. *International Journal for Numerical Methods in Fluids* 2002; **39**:247–275.
20. Zhou JG, Causon DM, Mingham CG, Ingram DM. The surface gradient method for the treatment of source terms in the shallow-water equations. *International Journal for Numerical Methods in Fluids* 2001; **168**:1–25.
21. Mingham CG, Causon DM. High-resolution finite-volume method for shallow water flows. *Journal of Hydraulic Engineering* 1998; **124**:605–614.
22. Frazão SS, Zech Y. Undular bores and secondary waves-experiments and hybrid finite-volume modelling. *Journal of Hydraulic Research* 2002; **40**:33–43.
23. Zhao DH, Shen HW, Tabios III GQ, Lai JS, Tan WY. Finite-volume two-dimensional unsteady-flow model for river basins. *Journal of Hydraulic Engineering* 1994; **120**:863–882.
24. Roe PL. Approximate Riemann solvers, parameter vectors, and difference schemes. *Journal of Computational Physics* 1981; **43**:357–372.
25. Wei G, Kirby JT. Time-dependent numerical code for extended Boussinesq equations. *Journal of Waterway*, *Port*, *Coastal*, *and Ocean Engineering* 1995; **121**:251–261.
26. Yamamoto S, Kano S, Daiguji H. An efficient CFD approach for simulating unsteady hypersonic shock-shock interference flows. *Computers and Fluids* 1998; **27**:571–580.
27. Abbott MB, Minns AW. *Computational Hydraulics* (2nd edn). Ashgate: USA, 1998.
28. Schäffer HA, Madsen PA. Discussion of 'A formal derivation and numerical modelling of the improved Boussinesq equations for varying depth'. *Ocean Engineering* 1998; **25:**497–500.
29. Beji S, Nadaoka K. Authors' reply to Discussion of Schäffer and Madsen on 'A formal derivation and numerical modelling of the improved Boussinesq equations for varying depth'. *Ocean Engineering* 1998; **25**:615–618.
30. Schäffer HA, Madsen PA. Further discussion related to 'A formal derivation and numerical modelling of the improved Boussinesq equations for varying depth' by Beji and Nadaoka. *Ocean Engineering* 1999; **26:**1057–1062.
31. Li YS, Liu S-X, Wai OWH, Yu Y-X. Wave concentration by a navigation channel. *Applied Ocean Research* 2000; **22**:199–213.
32. Abbott MB, Minns AW. *Computational Hydraulics* (2nd edn). Ashgate: USA, 1998.

DOI: 10.1002/fld